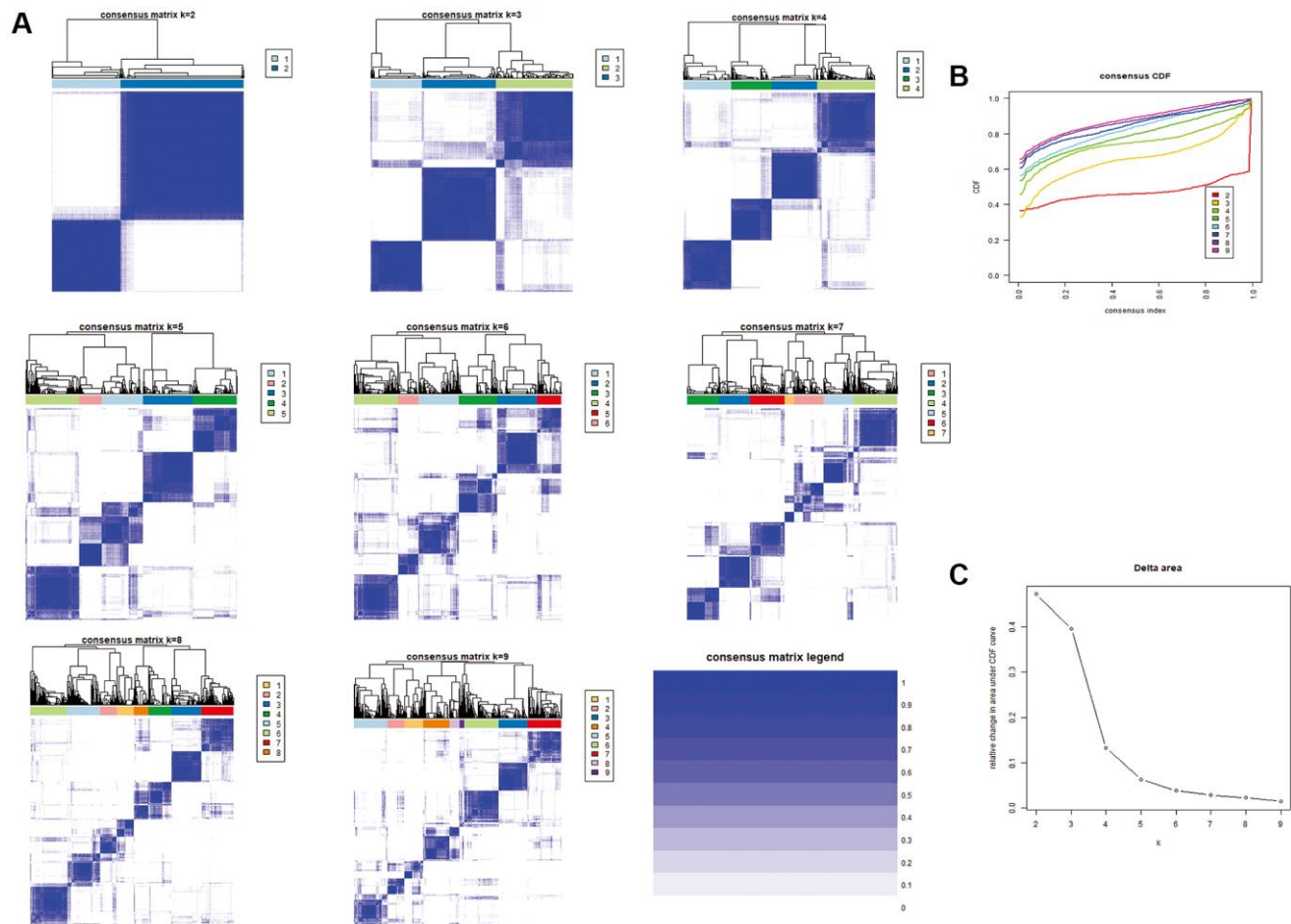
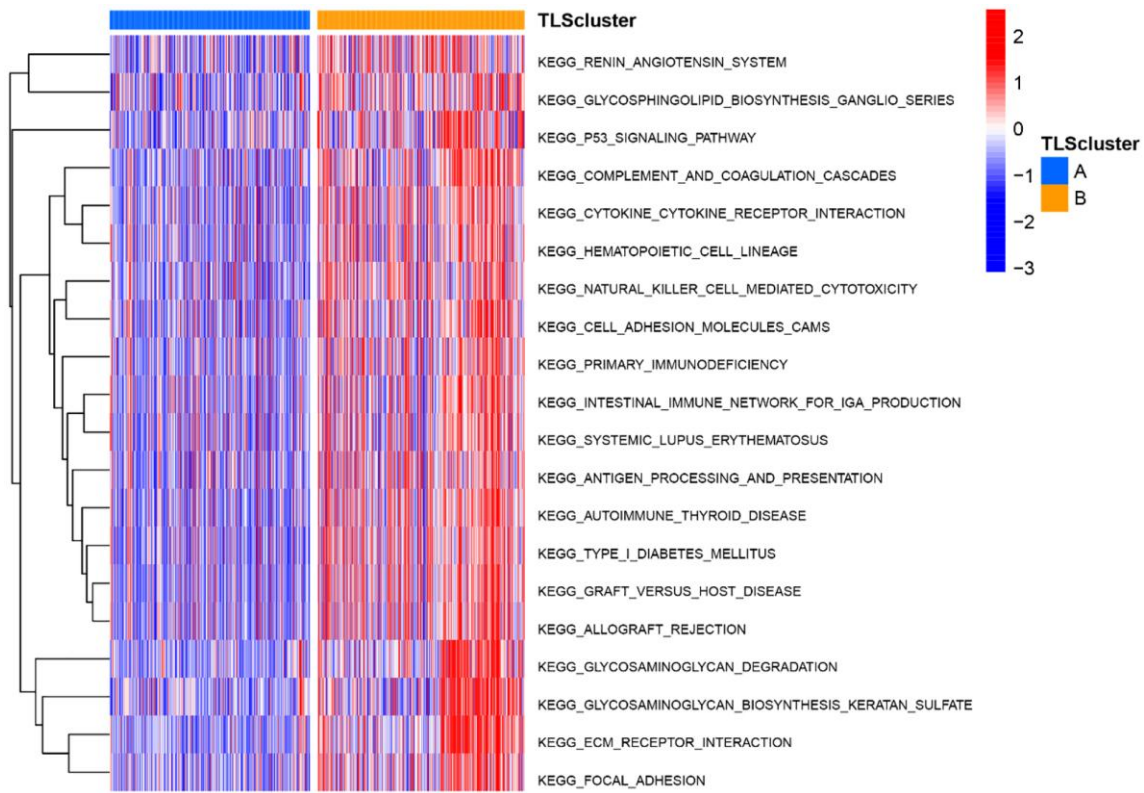


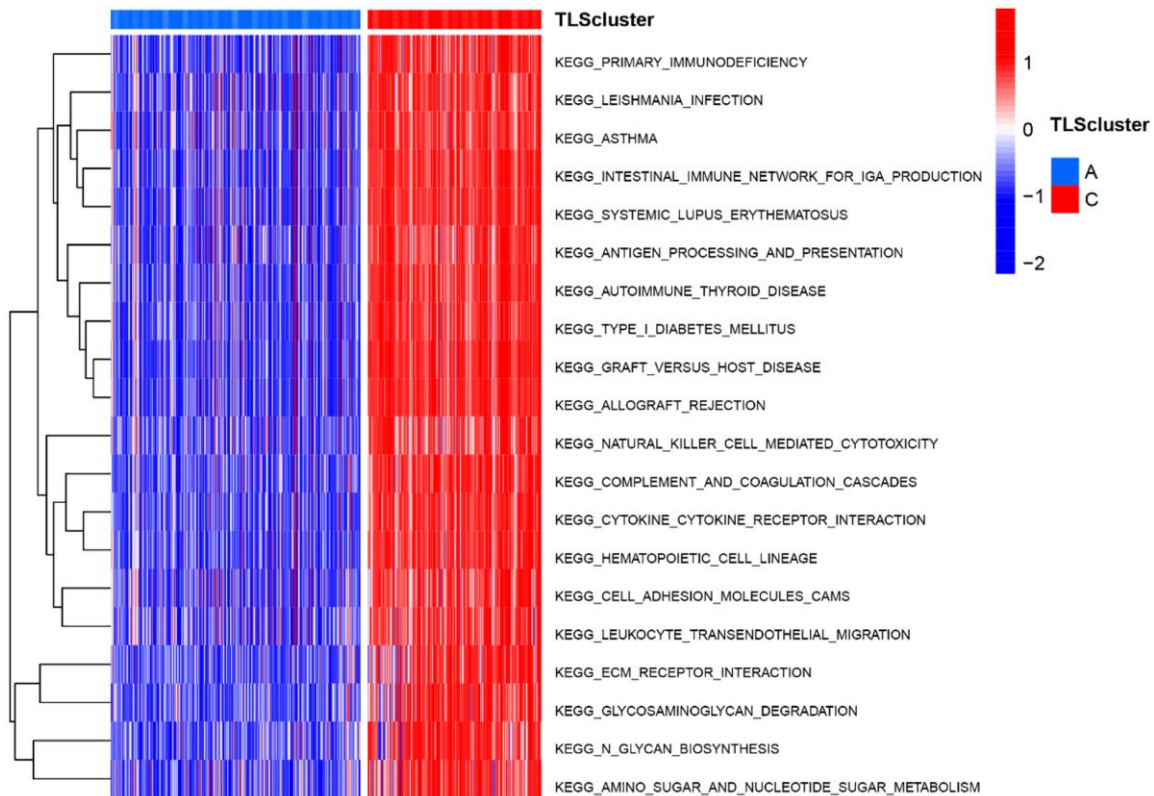
SUPPLEMENTARY FIGURES



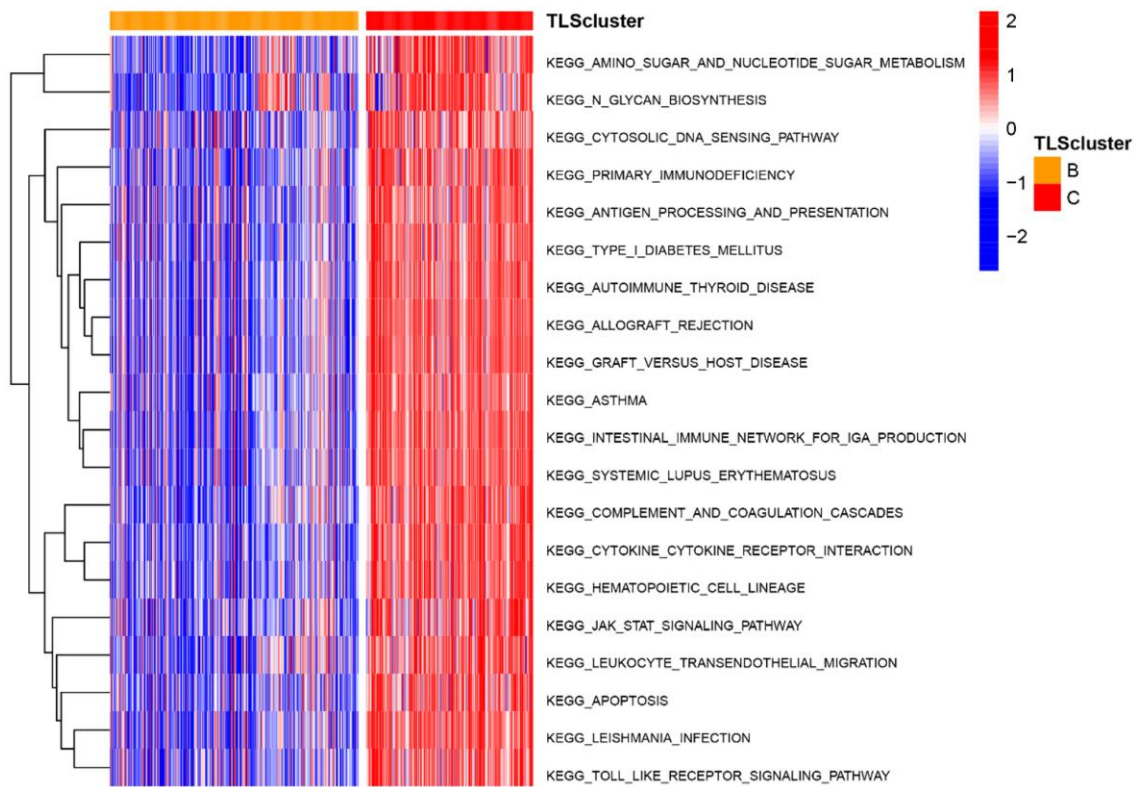
Supplementary Figure 1. Consensus clustering based in TLS gene expression of TCGA glioma. (A) Clustering matrix for $k = 2$ to $k = 9$. **(B)** CDF (cumulative distribution function) curve for $k = 2$ to $k = 10$. **(C)** Relative change in area under CDF curve for $k = 2$ to $k = 10$.



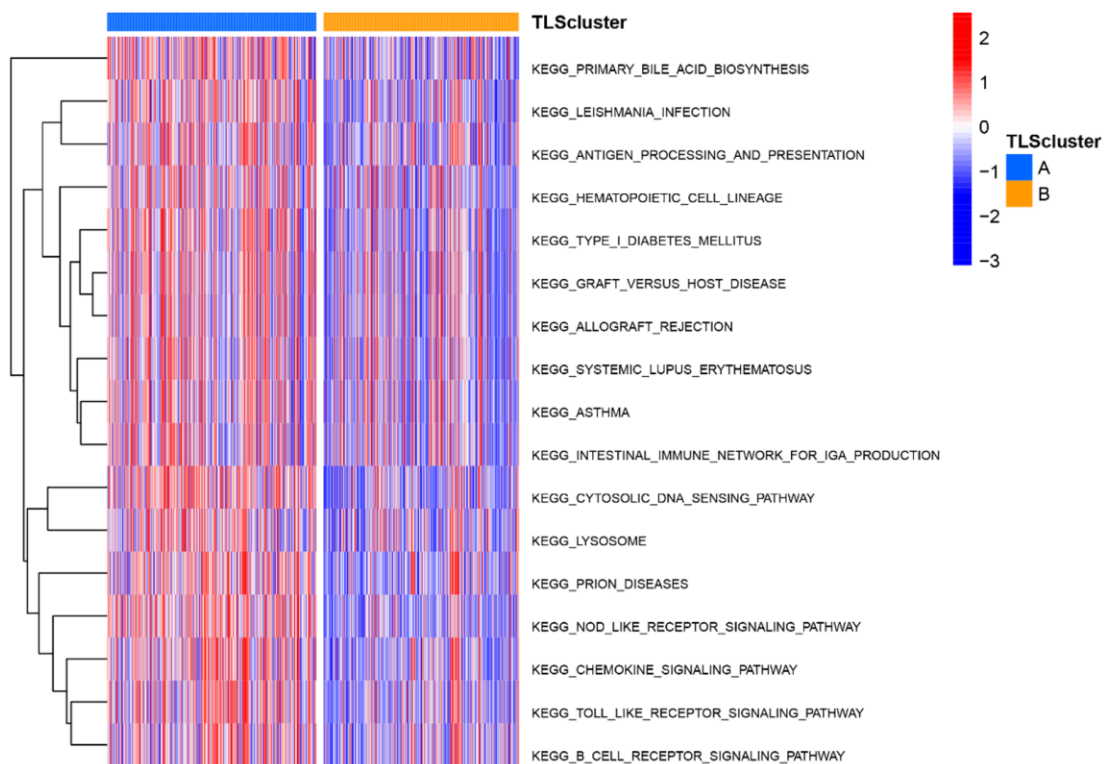
Supplementary Figure 2. The top 20 potential biological functions between subtype A and B in TCGA.



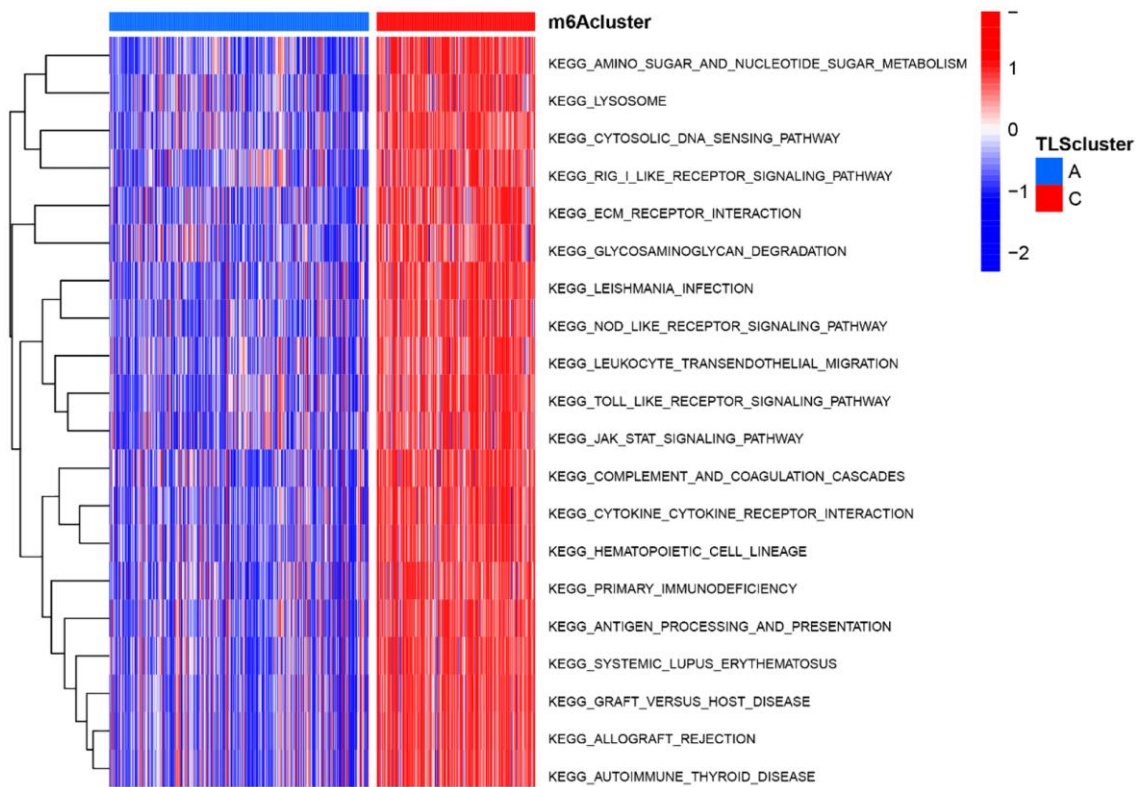
Supplementary Figure 3. The top 20 potential biological functions between subtype A and C in TCGA.



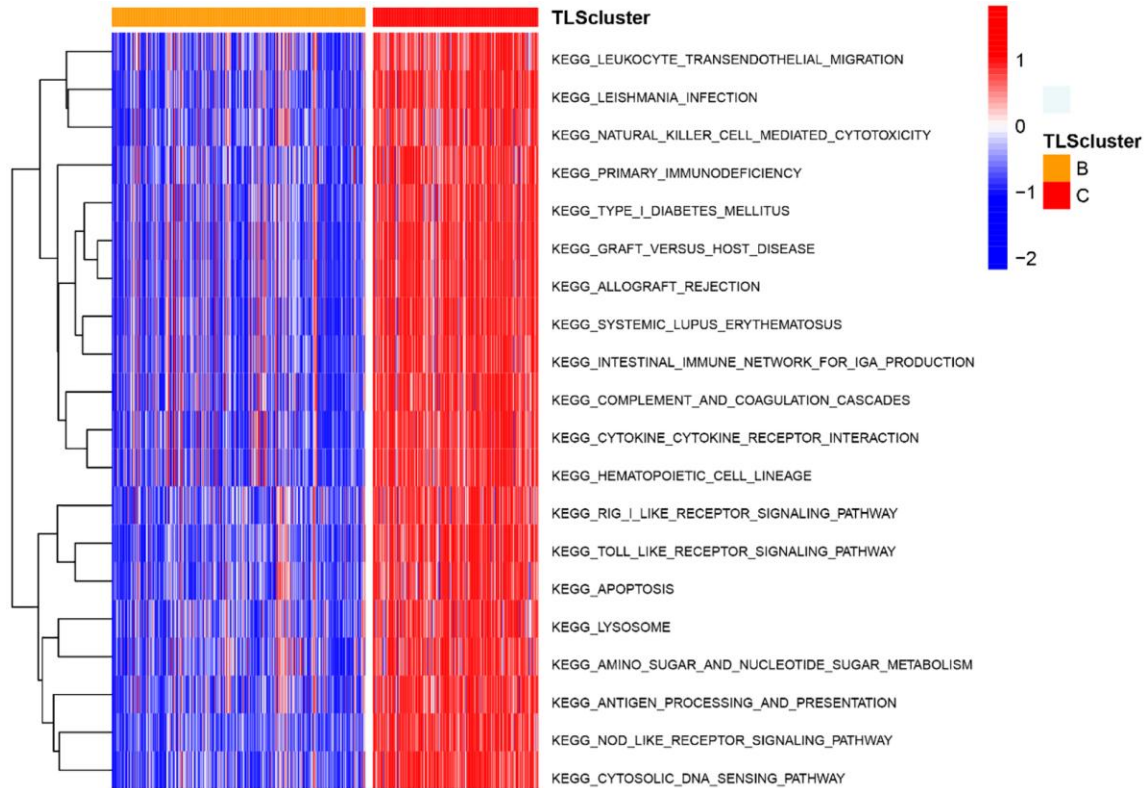
Supplementary Figure 4. The top 20 potential biological functions between subtype B and C in TCGA.



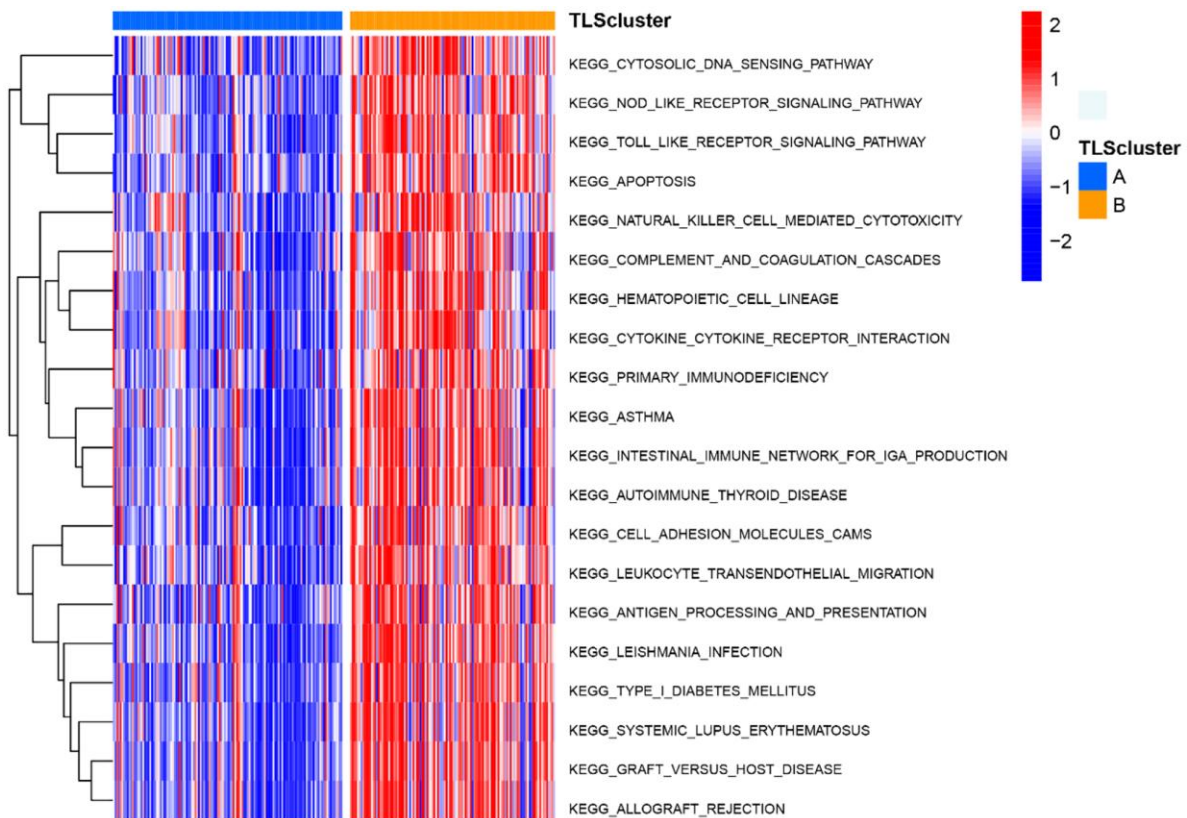
Supplementary Figure 5. The top 20 potential biological functions between subtype A and B in CGGA_cohort1.



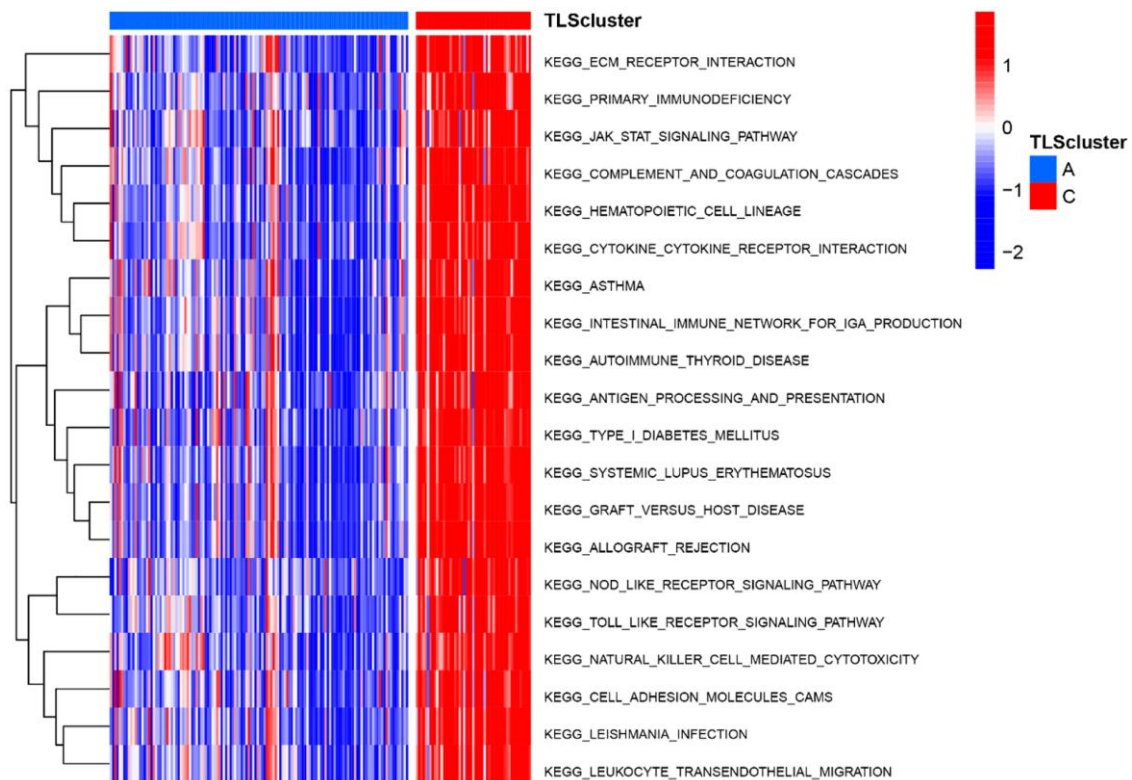
Supplementary Figure 6. The top 20 potential biological functions between subtype A and C in CGGA_cohort1.



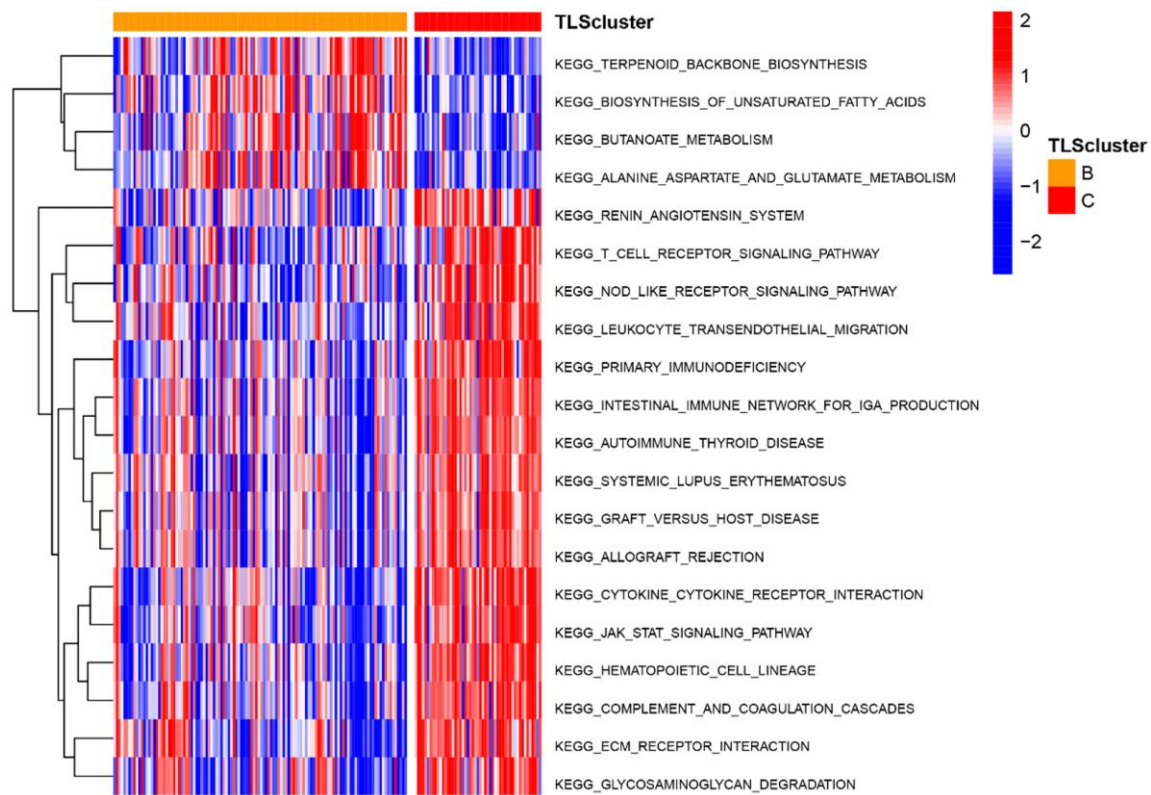
Supplementary Figure 7. The top 20 potential biological functions between subtype B and C in CGGA_cohort1.



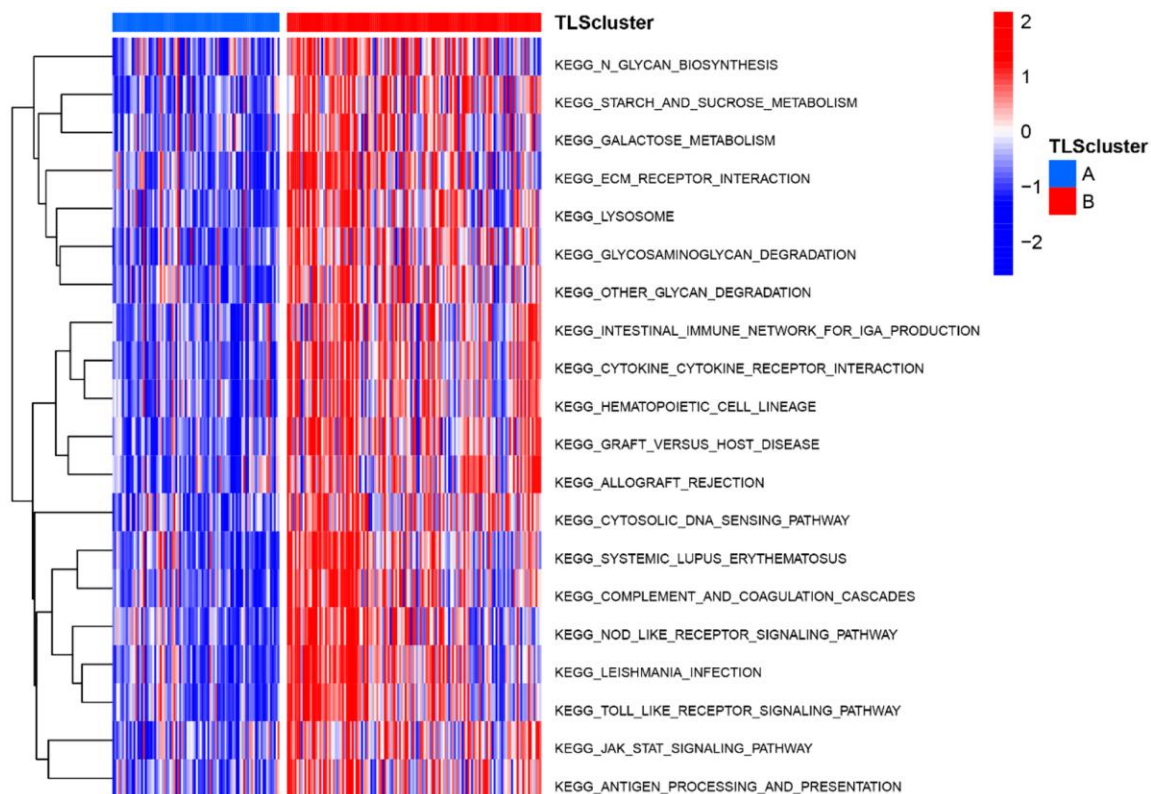
Supplementary Figure 8. The top 20 potential biological functions between subtype A and B in CGGA_cohort2.



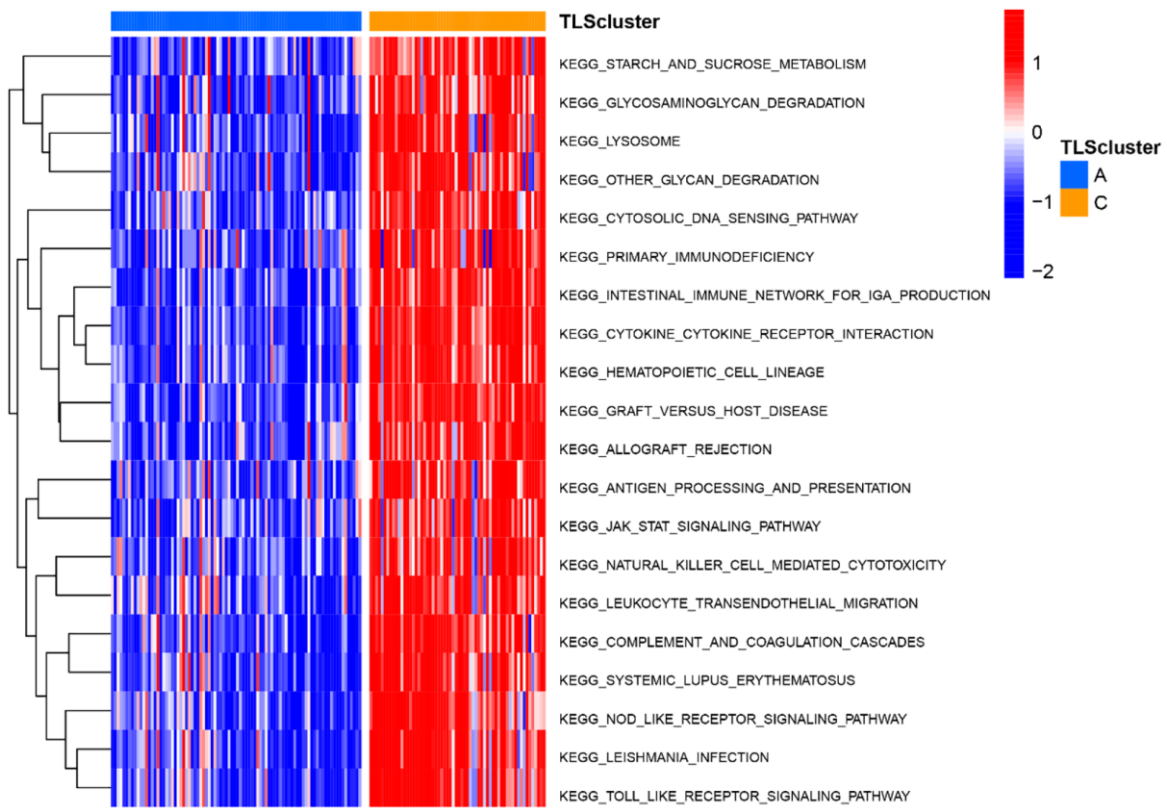
Supplementary Figure 9. The top 20 potential biological functions between subtype A and C in CGGA_cohort2.



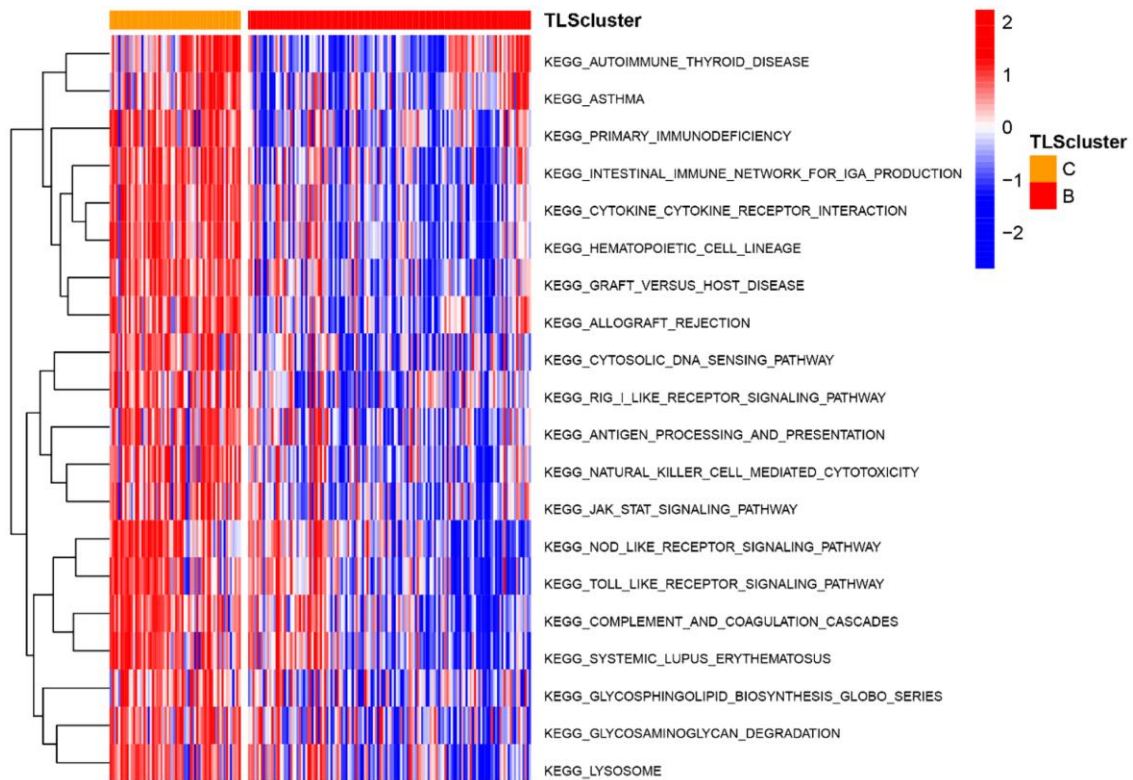
Supplementary Figure 10. The top 20 potential biological functions between subtype B and C in CGGA_cohort2.



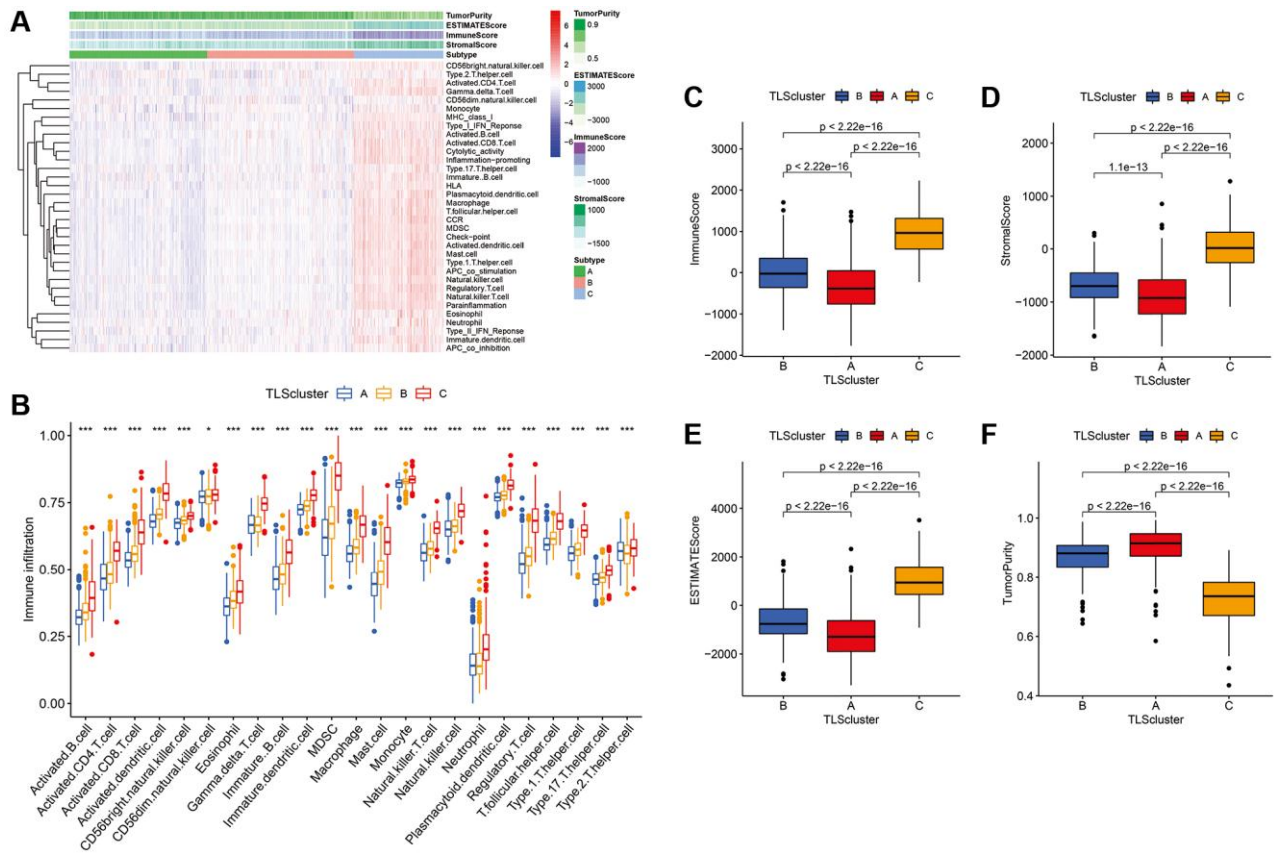
Supplementary Figure 11. The top 20 potential biological functions between subtype A and B in GSE16011.



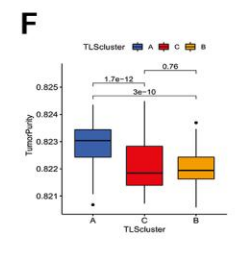
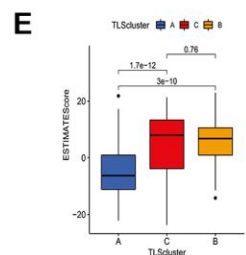
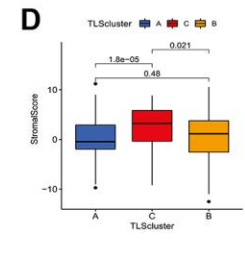
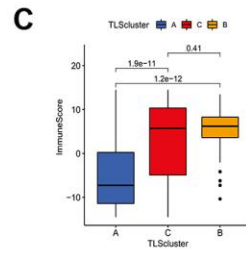
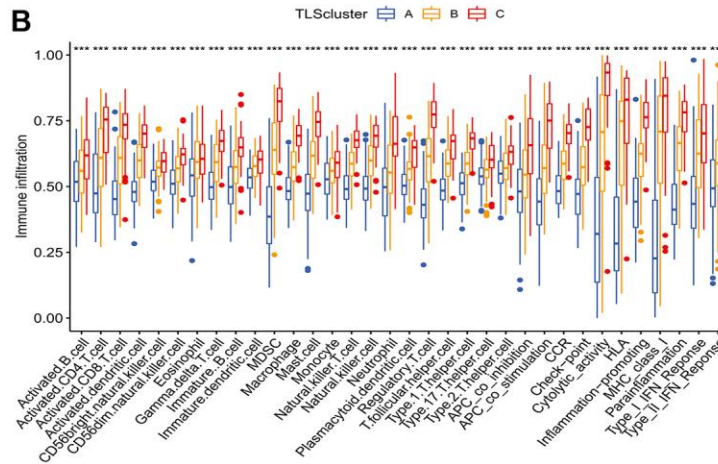
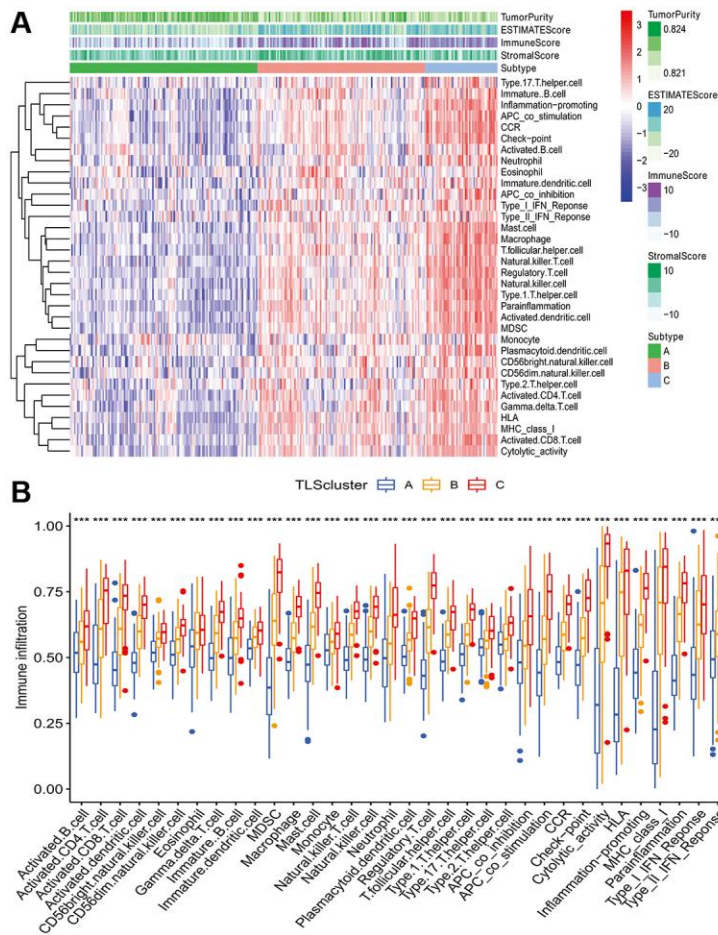
Supplementary Figure 12. The top 20 potential biological functions between subtype A and C in GSE16011.



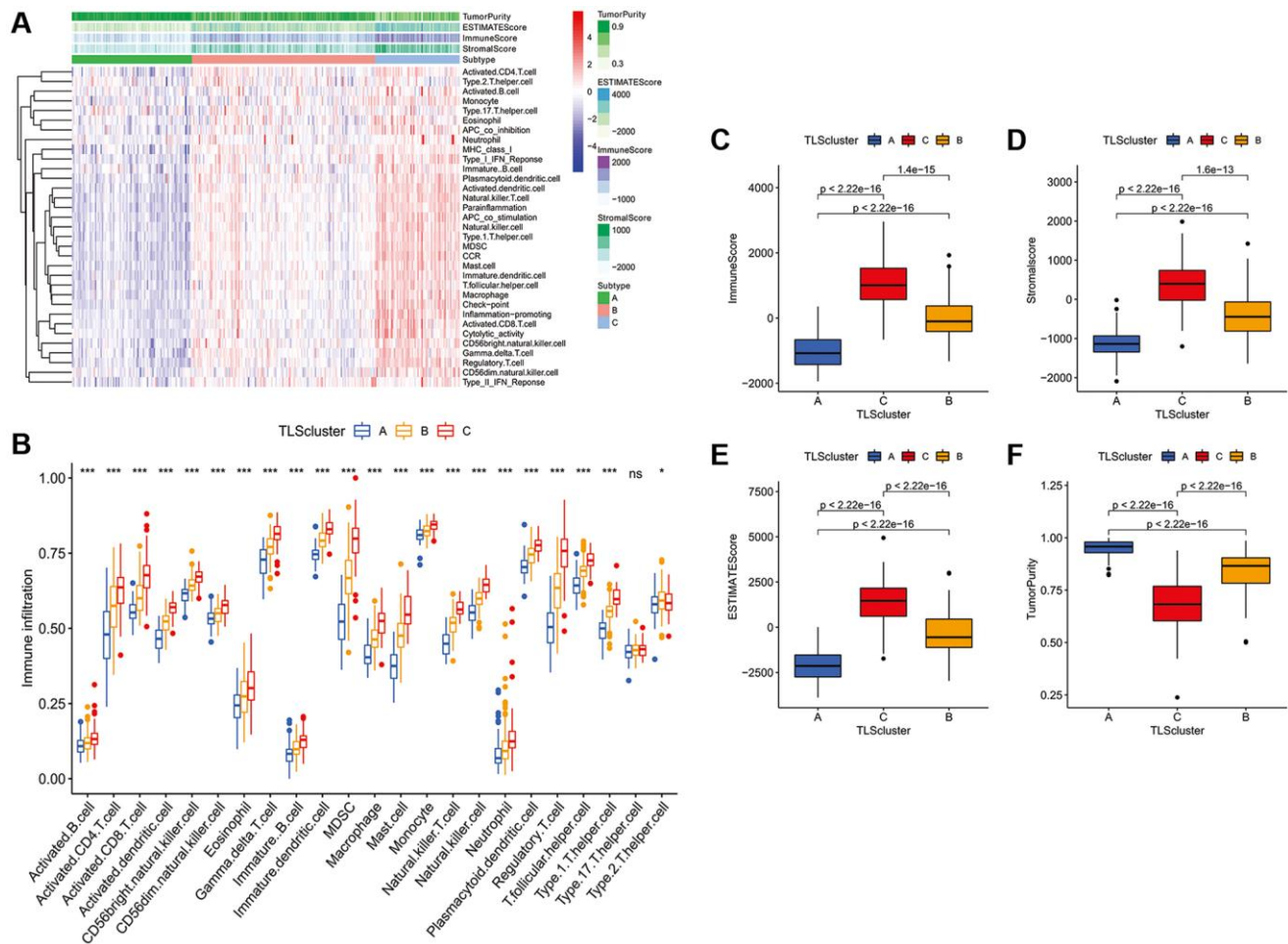
Supplementary Figure 13. The top 20 potential biological functions between subtype B and C in GSE16011.



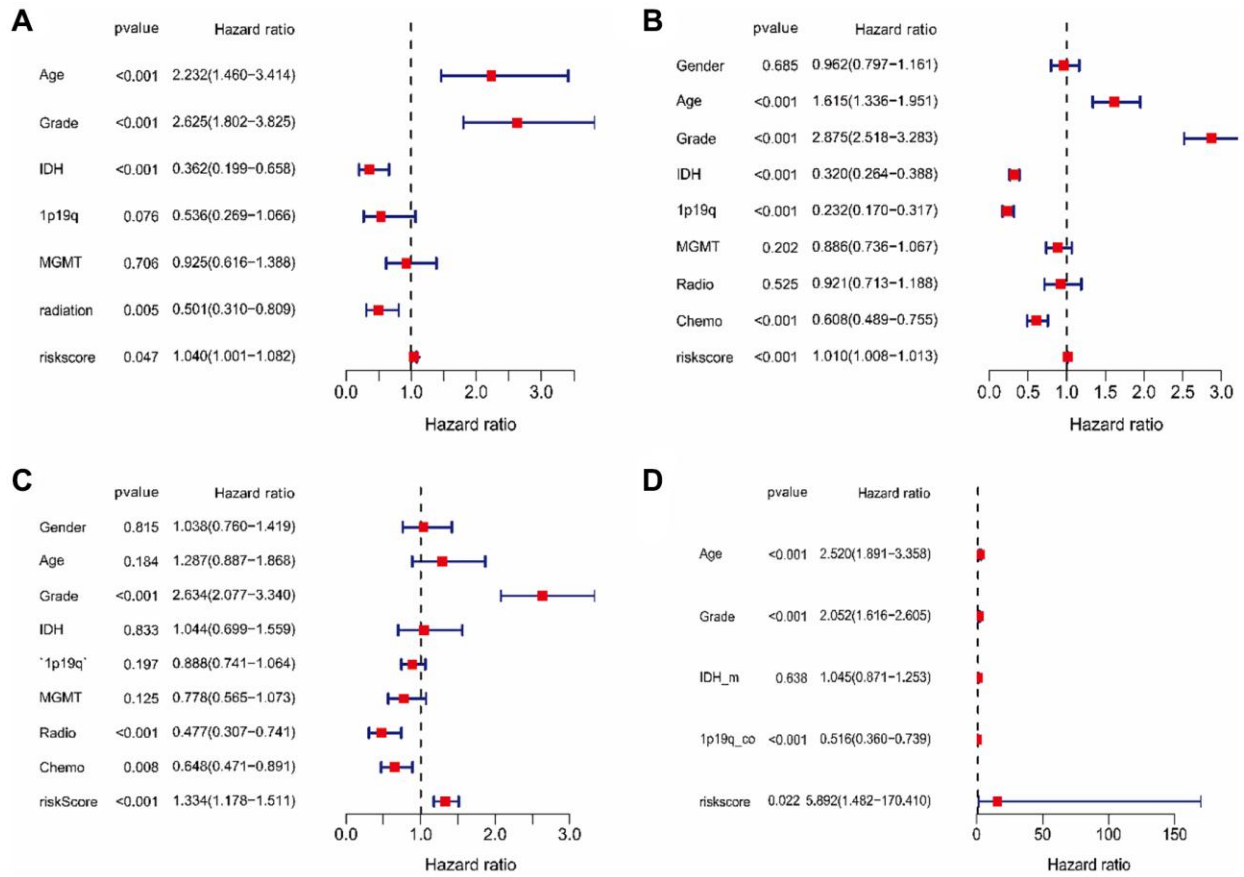
Supplementary Figure 14. Immune infiltration and tumor microenvironment of three metabolic subtypes in CGGA_cohort1. (A) Heatmap of TLS subtypes associated with immune infiltration and immune function. (B) The signature of 23 immune cell among TLS subtypes. (C–F) tumor microenvironment of TLS subtypes. C subtype had higher immune, stromal, and ESTIMATE scores compared with the scores of the A and B subtypes; however, tumor purity was lower.



Supplementary Figure 15. Immune infiltration and tumor microenvironment of three metabolic subtypes in CGGA_cohort2. (A) Heatmap of TLS subtypes associated with immune infiltration and immune function. (B) The signature of 23 immune cell among TLS subtypes. (C–F) tumor microenvironment of TLS subtypes. C subtype had higher immune, stromal, and ESTIMATE scores compared with the scores of the A and B subtypes; however, tumor purity was lower.



Supplementary Figure 16. Immune infiltration and tumor microenvironment of three metabolic subtypes in GSE16011. (A) Heatmap of TLS subtypes associated with immune infiltration and immune function. **(B)** The signature of 23 immune cell among TLS subtypes. **(C–F)** tumor microenvironment of TLS subtypes. C subtype had higher immune, stromal, and ESTIMATE scores compared with the scores of the A and B subtypes; however, tumor purity was lower.



Supplementary Figure 17. Multivariate Cox regression analysis of riskscore in TCGA cohort (A), CGGA_cohort1 (B), CGGA_cohort2 (C) and GSE16011 (D).